



Calibration method for a breast intervention robot based on four-dimensional ultrasound image guidance

Guo Yanjun¹ · Duan Xingguang¹ · Wang Chengyi² · Zhang Haicheng³ · Guo Huiqin⁴

Received: 30 December 2020 / Accepted: 9 July 2022 / Published online: 29 July 2022
© The Author(s) 2022

Abstract

In breast interventional ultrasound therapy, it is difficult to directly diagnose the location of a tumor in 2-D ultrasound images. To assist surgeons in treatment more intuitively, a four-dimensional ultrasound image-guided breast intervention robot is proposed. The calibration approach of the ultrasonic image for the robot is one of the main contents of the research. This method is based on the establishment of a complete coordinate system conversion model, and it uses the ORB (oriented FAST and rotated BRIEF) feature extraction method to obtain and record the real-time image marker pixel positions, calculate the unknown parameters of the coordinate system conversion matrix, and establish a complete calibration system. This article demonstrates the feasibility of the calibration approach through experiments in our developed US-guided robotic system. Additional experimental and parametrical comparisons of the proposed method with state-of-the-art methods were conducted to thoroughly evaluate the outperformance of the proposed method.

Keywords Breast intervention robot · ORB features · Skin surface marking · US calibration

1 Introduction

In recent years, with the continuous advancement of medical ultrasound (US) imaging technology and its outstanding advantages, US images have become the main diagnostic and treatment tool for breast lesions. US image-guided surgery

has been used successfully in the auxiliary diagnosis and treatment of breast cancer, which is usually called interventional ultrasound (Solbiati & Tondolo, 2013). It is difficult for the surgeons to directly diagnose the location of a tumor in 2-D US images. Therefore it is necessary to reconstruct breast tumors to overcome the limitations of 2-D US imaging (Papenberg et al., 2008). Due to the shape of breast is prone to change in real-time during the surgery, the mapping of the US image frame and the patient frame changes in real-time, a reconstruction of the 4-D breast model, which shows the 3-D breast model in a moving state, is more suitable for clinical application of breast US intervention therapy.

To implement of breast US intervention treatment guided by 4-D US image, it is first necessary to convert the imaging frame to the surgical frame (original coordinate system), which is called the calibration of the US image. In the past ten years, scholars around the world have successfully researched calibration approaches and the corresponding optimization algorithms. Mostly, the US image calibration requires a phantom to provide a set of fiducials, e.g. the N-wire phantom method (Carbajal et al., 2013) and multi-wedge phantom method (Najafi et al., 2014), they are traditional US calibration methods. With the development of surgical robots, the traditional calibration methods no longer meet the clinical application, therefore some US image calibra-

✉ Guo Yanjun
gmy63000@126.com

Duan Xingguang
duanstar@bit.edu.cn

Wang Chengyi
wangcy@radi.ac.cn

Zhang Haicheng
haichengzhang@bjmu.edu.cn

Guo Huiqin
1917216708@qq.com

- ¹ Beijing Institute of Technology, Haidian District, Beijing, China
- ² Institute of Remote Sensing and Digital Earth, Chinese Academy of Sciences, Haidian District, Beijing, China
- ³ Peking University People's Hospital, Xicheng District, Beijing, China
- ⁴ Chengcheng County Hospital, Weinan City, Shanxi Province, China

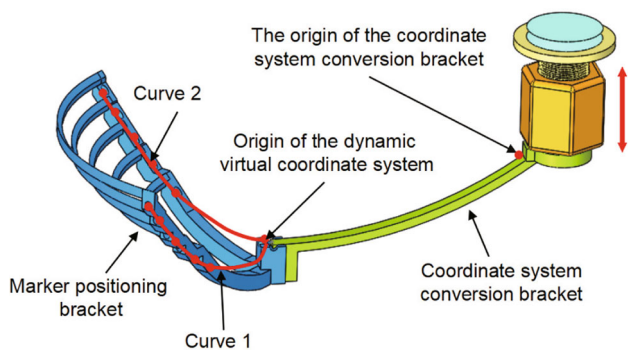


Fig. 2 Dynamic calibration phantom bracket

For the proposed calibration approach, a 4-D dynamic calibration phantom was designed and applied to the US image calibration for a breast intervention robot. The functions and components of the 4-D dynamic calibration phantom bracket include a marker positioning bracket with marking holes, a coordinate system conversion bracket, an adjustable screw and nut, and a double-sided suction cup, as shown in Fig. 2. The coordinate system of the patient’s breast is defined as the virtual coordinate system in the calibration approach, and the center of the nipple is set as the origin of the virtual coordinate system. The positions of the marking holes on the positioning bracket are evenly arranged on two flat arc curves, and the marking holes are processed by precision instruments. The parameters of the coordinate conversion between the conversion bracket and the virtual coordinate system are determined by the size and structure of the conversion bracket. The red double arrow indicates the direction in which the dynamic phantom can be moved and adjusted, and the two red curves indicate the locations of the markers.

Before calibration, the registration of US probe and operating table in the optical navigation system is completed, and the mappings between US probe, operating table and optical navigation system are established. The specific procedures for registration are as follows: (1) The passive rigid body is fixed at the center of US probe, and the optical positioner tracks its position and posture. The coordinate system of US probe is set as O_S , the coordinates origin is the center of US probe, and the XOY plane is parallel to US imaging plane. The coordinate system of US image is set as O_I , the coordinates origin is at the upper left corner of US image, and the UOV plane coincides with US image plane. Therefore, there is only translation without rotation between US image and US probe. (2) The NDI navigation system detects the coordinate origin of coordinate transformation bracket fixed on operating table through passive 4-point probe and records its position information. The operating table is placed horizontally, and the patient lying prone on it. Therefore, the XOY plane of operating table is parallel to horizontal plane, and

there is only translation between operating table and optical navigator.

In the overall frame of US calibration, five coordinate systems are defined: the US image, the actual and virtual coordinates of the coordinate conversion bracket, the US probe, and the NDI optical navigator, which are presented as $I, M', M, S,$ and $R,$ respectively. The four corresponding coordinate transformation matrices are $T_I^S, T_S^R, T_R^{M'}, T_{M'}^M$.

3 Skin surface marker

The patient’s breast surface is used as the carrier of the markers. Before the operation, the doctor adjusts the conversion bracket fit to the patient’s position and shape so that the intersection of the curve on the marker positioning bracket coincides with the origin of the virtual coordinate system, then uses the marker positioning bracket to mark the skin surface of patient’s breast, as shown in Fig. 3.

The marker is a small steel ball with a diameter of 2 mm. A total of eight markers are divided into two groups, four in each group, and fixed on breast skin surface with glue. The sticking position of marker on breast surface is determined through graduation hole on the marker positioning bracket. Curves C_1 and C_2 intersect at right angles in space, and intersection point is O_M . Intersection of two planes is set as the Z axis of virtual coordinate system. The virtual dynamic coordinate system changes in real time with the position and shape of breast during operation. In the US probe calibration, US probe scans these two cross-sections located by the two curves, as well as NDI optical navigator detects the position of US probe.

We construct a cylindrical coordinate system in the dynamic calibration phantom: O_M is the coordinates origin, and Z axis is the center of cylindrical coordinate system. The coordinates of a point in the dynamic virtual rectangular

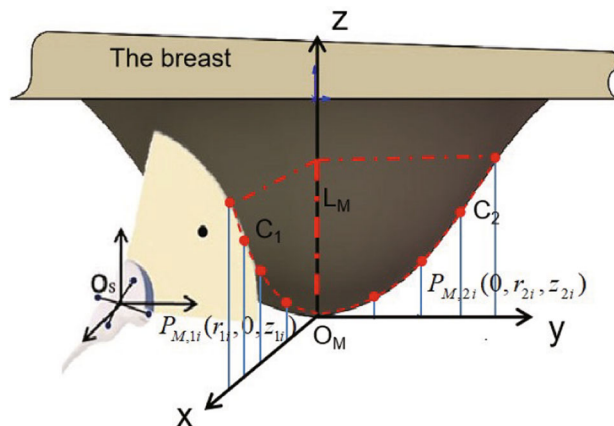


Fig. 3 Markers on the skin surface of breast

coordinate system of the breast can be expressed as $P_M = [x_m \ y_m \ z_m]^T$. We convert P_M from cylindrical coordinates to rectangular coordinates: $P_M = [r \cos \psi \ r \sin \psi \ z]^T$, and the initial angular coordinates ψ of markers on curves C_1 and C_2 are $\psi_1 = 0^\circ$ and $\psi_2 = 90^\circ$, respectively. The coordinates of markers on curves C_1 and C_2 can be obtained as $P_{M,1i} = (r_{1i}, 0, z_{1i})$ and $P_{M,2i} = (0, r_{2i}, z_{2i})$, $i = 0, 1, 2, 3$.

4 Mathematical model for dynamic US calibration approach

The space mapping of a point from the US image to the patient’s breast is expressed as follows:

$$P_M = T P_I = T_{M'}^M (T_{M'}^R)^{-1} T_S^R T_I^S P_I \tag{1}$$

P_I represents the position of a point in US image. If the thickness of US probe is p mm, then $P_I = [u \ v \ -\frac{p}{2}]^T$, $p \in [8, 10]$, u and v are the position of the point with the unite of pixel.

Matrix $T_{M'}^M$ is the transformation matrix from operating table frame to breast frame. The translation parameters are determined by the structure and size of coordinate conversion bracket. Suppose the translation parameters are $(x_1, y_1, z_1) = (0, 100, 30)$ and the units are mm. Assuming that quaternion parameter of the rotation transformation is (w_1, a_1, b_1, c_1) in $T_{M'}^M$, the specific expression is as follows (Yi et al., 2009):

$$T_{M'}^M = \begin{bmatrix} 1-2b_1^2-2c_1^2 & 2a_1b_1-2c_1w_1 & 2a_1c_1+2b_1w_1 & 0 \\ 2a_1b_1+2c_1w_1 & 1-2a_1^2-2c_1^2 & 2b_1c_1-2a_1w_1 & 100 \\ 2a_1c_1-2b_1w_1 & 2b_1c_1+2a_1w_1 & 1-2a_1^2-2b_1^2 & 30 \\ 0 & 0 & 0 & 1 \end{bmatrix} \tag{2}$$

The rotation parameters $[w_1 \ a_1 \ b_1 \ c_1]^T$ change in real time in the 4-D dynamic calibration phantom. According to conventional and intuitive method of expressing rotation, we introduce a rotation vector $\vec{k} = [x \ y \ z]^T(t)$ and a rotation angle $\theta(t)$, which represents the rotation angle of coordinate system M around axis vector \vec{k} at time t . Finally, the rotation of breast coordinate system is represented as,

$$[w_1 \ a_1 \ b_1 \ c_1]^T(t) = [\cos \frac{\theta}{2} \ x \ \sin \frac{\theta}{2} \ y \ \sin \frac{\theta}{2} \ z \ \sin \frac{\theta}{2}]^T(t) \tag{3}$$

In the process of calibration, the rotation angle θ changes in real time with breast movement and deformation, and the real-time dynamic rotation parameters $\theta, x, y,$ and z will be solved by PSO algorithm.

Transformation matrix $T_R^{M'}$ represents translation transformation between NDI optical navigator frame and template

support frame. We use passive 4-marker probe to detect the position of coordinate origin of phantom holder to obtain the translation $[x_{m'} \ y_{m'} \ z_{m'} \ 1]^T$. Then, the translation transformation matrix is,

$$T_{M'}^R = \begin{bmatrix} 1 & 0 & 0 & -x_{m'} \\ 0 & 1 & 0 & -y_{m'} \\ 0 & 0 & 1 & -z_{m'} \\ 0 & 0 & 0 & 1 \end{bmatrix} \tag{4}$$

Conversion matrix T_S^R represents the coordinate system conversion between NDI optical navigator frame and US probe frame. The posture of passive rigid body recorded by the NDI is in form of quaternion; therefore, T_S^R has a total of 7 parameters, four of which are rotation parameters and three of which are displacement parameters, which are $[w_2 \ a_2 \ b_2 \ c_2 \ x_2 \ y_2 \ z_2]$.

$$T_S^R = \begin{bmatrix} 1-2b_2^2-2c_2^2 & 2a_2b_2-2c_2w_2 & 2a_2c_2+2b_2w_2 & x_2 \\ 2a_2b_2+2c_2w_2 & 1-2a_2^2-2c_2^2 & 2b_2c_2-2a_2w_2 & y_2 \\ 2a_2c_2-2b_2w_2 & 2b_2c_2+2a_2w_2 & 1-2a_2^2-2b_2^2 & z_2 \\ 0 & 0 & 0 & 1 \end{bmatrix} \tag{5}$$

In the process of calibration, US probe scans the cross-sections where the two curves are located. Therefore, NDI optical navigator records two sets of pose information of US probe, corresponding conversion matrices in these two states are represented as $T_S^{R(1)}$ and $T_S^{R(2)}$.

The transformation equation from US image frame to US probe frame is,

$$\begin{bmatrix} x_s \\ y_s \\ -\frac{p}{2} \\ 1 \end{bmatrix} = T_I^S \begin{bmatrix} u \\ v \\ -\frac{p}{2} \\ 1 \end{bmatrix} = \begin{bmatrix} -\frac{1}{\alpha} & 0 & 0 & -\frac{c_x}{\alpha} \\ 0 & \frac{1}{\beta} & 0 & -\frac{c_y}{\beta} \\ 0 & 0 & 1 & 0 \\ 0 & 0 & 0 & 1 \end{bmatrix} \begin{bmatrix} u \\ v \\ -\frac{p}{2} \\ 1 \end{bmatrix} \tag{6}$$

T_I^S is the transformation matrix from US image to US probe frame. The pixel coordinates are scaled α times on the u axis and β times on the v axis. In general, $\alpha = \beta = 0.1148$, the units are pixels per millimeter, and the origin is shifted by $[c_x, c_y]^T = [19, 19]^T$; the units are pixels. So the transformation matrix is obtained by, $T_I^S =$

$$\begin{bmatrix} -8.71 & 0 & 0 & -165.51 \\ 0 & 8.71 & 0 & -165.51 \\ 0 & 0 & 1 & 0 \\ 0 & 0 & 0 & 1 \end{bmatrix}$$

Substituting P_I and P_M into (1), we obtain,

$$\begin{bmatrix} r_{1i} \\ 0 \\ z_{1i} \\ 1 \end{bmatrix} (t) = T_{M'}^M(t) \cdot T_R^{M'} \cdot T_S^{R(1)} \cdot T_I^S \cdot \begin{bmatrix} u_{1i} \\ v_{1i} \\ -\frac{p}{2} \\ 1 \end{bmatrix} (t) \tag{7}$$

$$\begin{bmatrix} 0 \\ r_{2i} \\ z_{2i} \\ 1 \end{bmatrix} (t) = T_M^M(t) \cdot T_R^{M'} \cdot T_S^{R(2)} \cdot T_I^S \cdot \begin{bmatrix} u_{2i} \\ v_{2i} \\ -\frac{P}{2} \\ 1 \end{bmatrix} (t) \quad (8)$$

Expanding the zero elements on the left side of the two linear matrix equations, we obtain two equations below, which represent the calibration models of two poses of US probe; f_1 and f_2 represent the calibration equations when US probe scans curves C_1 and C_2 , respectively.

$$\begin{cases} f_{1,i}(\theta, x, y, z) = 0 \\ f_{2,i}(\theta, x, y, z) = 0 \end{cases} \quad (9)$$

The parameters of transformation matrix in the US calibration approach are $\theta, x, y,$ and z , which will be solved in our research.

If the cycle of compound movement of patient’s breast, which moves with breathing, heart beating and artery motion, is T , then $0 \leq t \leq T$. US image sequences I_1 and I_2 are acquired in this compound motion cycle to obtain original image data set of markers. ORB method is used to extract the feature points of markers from the two sets of image sequence and obtain the pixel positions of markers. At the same time, NDI optical navigator records the pose information $T_S^{R(1)}$ and $T_S^{R(2)}$ of two states of US probe and calculates the conversion matrix between US image and patient’s breast frame through above mathematical model.

5 Solution of initial rotation parameters

In the proposed US image calibration, PSO algorithm is used to solve the dynamic rotation parameters. The main contents of this algorithm is summarized as follows:

1. The parameters $\theta, x, y,$ and z are defined as the dimensional variables x_{ji} of PSO, where $j = 1, 2, \dots, N;$ $i = 0, 1, 2, 3$. The ranges of particle positions are $0 \leq x_{j0} = \theta \leq \pi, 0 \leq x_{j1} = x \leq 1, 0 \leq x_{j2} = y \leq 1, 0 \leq x_{j3} = z \leq 1$.
2. Initialize the single extremum $p_{ji} = x_{ji}(0)$ of the particle, and global extremum p_{gi} is determined by one particle which has the smallest fitness value among the N particles.
3. Evolution equations for particle velocity and position are,

$$v_{ji}(s + 1) = \omega v_{ji}(s) + c_1 r_1(s) [p_{ji}(s) - x_{ji}(s)] + c_2 r_2(s) [p_{gi}(s) - x_{gi}(s)] \quad (10)$$

$$x_{ji}(s + 1) = x_{ji}(s) + v_{ji}(s + 1) \quad (11)$$

4. The fitness function of PSO algorithm for the US calibration is defined as,

$$F(X) = \sum_{i=0}^3 (f_{1,i}^2(x) + f_{2,i}^2(x)) \quad (12)$$

5. Calculate the fitness $F(x)$ of each particle, update the particle position with PSO iterative algorithms, select and update the global optimal position.
6. When does the iteration terminate is determined by $\xi = |F(x) - \hat{F}(x)| = |F(x)| \leq 0.001$.

6 Experiments and results

6.1 Materials and equipments

In order to verify the accuracy of dynamic US calibration, experiments are completed on breast intervention robotic system proposed by us, and a self-designed dynamic calibration phantom is used to calibrate US image. All structural parts of phantom are printed using a fused deposition modeling printer, polylactic acid (PLA) is used as the materials. Use the phantom to paste two groups of markers on patient’s breast skin surface, each group contain 4 ones, a total of 8 markers, and the processing accuracy of positioning holes and markers reaches 0.1mm. Measure the angle values of two groups of markers in the phantom frame with a universal bevel protractor. The positions of each markers in the phantom frame is recorded in Table 1.

The B-mode ultrasound, type LOGIQ P7, is produced by GE with a supporting image capture function. It can collect and transmit US images to the image workstation in real time through a video transmission port.

The NDI Polaris Spectra optical navigator, made in Canada, is used to track the pose of the US probe and transmit the signal of the pose data collected by the NDI optical navigator to the graphics workstation as the input information of the optimization algorithm. Obtain the position of coordinate conversion bracket by NDI optical navigator, it’s $[277.31 \ -235.02 \ -2217.08 \ 1]^T$, then substituted it into equation (4) to get the transformation matrix T_M^R .

NDI optical navigator record the postures of US probe in the two direction are

Table 1 Coordinates, P_M (mm), of markers in calibration phantom

Number	Marker 1	Marker 2	Marker 3	Marker 4
Curve C1	(82,0,41)	(74,0,33)	(66,0,25)	(58,0,17)
Curve C2	(0,82,41)	(0,74,33)	(0,66,25)	(0,58,17)

$$\begin{bmatrix} 0.5822 & -0.3791 & 0.7014 & 0.1651 & 224.74 \\ -206.98 & -2230.78 & & & \\ 0.4582 & -0.6413 & 0.4758 & 0.3966 & 237.19 \\ -161.36 & -2213.42 & & & \end{bmatrix}$$
 and

$$\begin{bmatrix} 0.4582 & -0.6413 & 0.4758 & 0.3966 & 237.19 \\ -161.36 & -2213.42 & & & \end{bmatrix}$$
, substitute them into equation (5) respectively to get the transformation matrixes $T_S^{R(1)}$ and $T_S^{R(2)}$.

The Dell Graphics Workstation is used to extract the feature of markers in US images and to run the optimization program and calibration application program.

In the master-slave control system of UR5 robot, the effector of the robot holds US probe, the master site of it is the Omega.6.

6.2 Image acquisition of markers on breast surface

Human breathing cycle is approximately 3 ~ 3.7 seconds, and the breathing cycle of patient in this experiment is $T = 3$ seconds. In two consecutive breathing cycles, Omega.6 as the master site is used to control UR5 robot holding US probe to scan the cross-section of patient’s breast and obtain US image sequences I_1 and I . The equipments, materials and processes used in the experiment are shown in Fig. 4.

The US image acquisition frequency is set to 30, and then 90 frames of serial images are acquired in period T. The US image of markers is shown in Fig. 5. The metal markers cause artifacts in the image, they are highlighted in the US image.

6.3 Position extraction of markers

The ORB method is used to extract the features of markers in this experiment, as ORB feature is currently a very representative real-time image feature. ORB maintains the

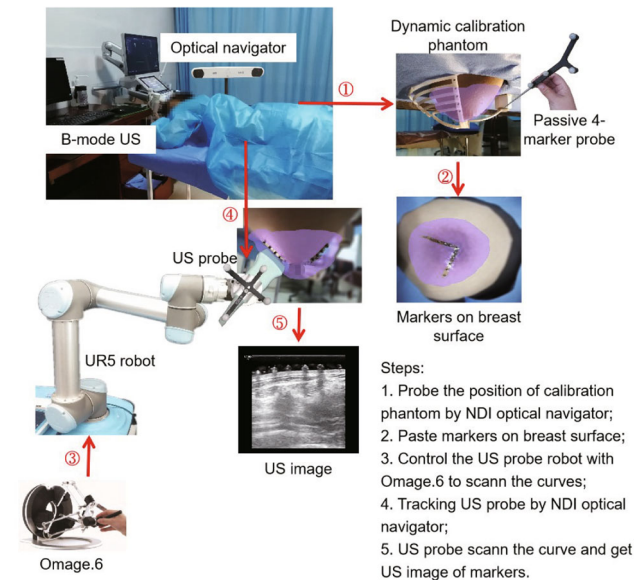


Fig. 4 Procedure of dynamic US calibration

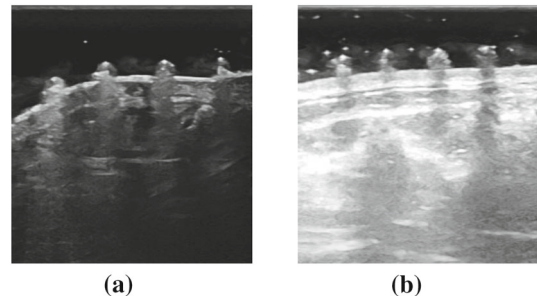


Fig. 5 Marker ultrasound images. The picture a is the image sequence I_1 , and the picture b is the image sequence I_2

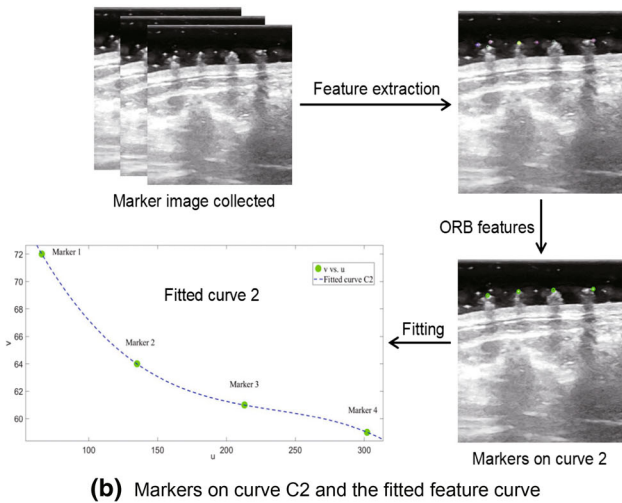
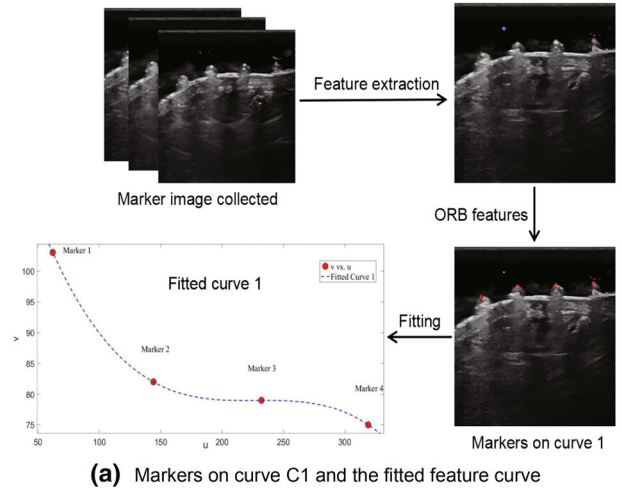


Fig. 6 ORB features and fitted feature curve in the sequence images

Table 2 Pixel positions, P_i (pixel), of the markers

Number	Marker 1	Marker 2	Marker 3	Marker 4
Curve C1	(62, 103)	(144, 82)	(232, 79)	(319, 75)
Curve C2	(66, 72)	(135, 64)	(213, 61)	(302, 59)

invariance of the rotation scale of the feature and has a significant increase in speed (Gupta et al., 2019). To completely extract the 4 markers from each sequence image, the number of ORB features is set to 10 in ORB algorithm. The coordinates of the highlights in the sequence image were extracted, there may be multiple very close highlights at one marker, remove them appropriately and calculate their average value. The result are shown in red and green circle marks, and the fitted feature curve are shown in Fig. 6, and their pixel positions are recorded in Table 2.

6.4 Solution of the calibration matrix

First, substitute the obtained $P_M, T_{M'}^R, T_S^{R(1)}, T_S^{R(2)}$, and P_I into (7) and (8), then according to (9), a equation set containing 4 target parameters is obtained, and a fitness function, which is introduced in PSO algorithm, is constructed with this equation set. The particle population size is set to $N = 50$, and the evolution parameters of particle velocity and position are set to $\omega = 0.8, c_1 = c_2 = 0.5$. Solve the target parameters through PSO and obtain:

$$B \Rightarrow \begin{cases} \theta = 7.2^\circ \\ x = 0.052 \\ y = 0.044 \\ z = 0.011 \end{cases}$$

Substitute the B into (2) and (3) to obtain $T_{M'}^M$, then substitute $T_{M'}^M, T_{M'}^R, T_S^{R(1)}$, and T_I^S into (1) to get the mapping from US image frame to patient’s breast frame on direction of curve 1(C1), in a similar way, to get the mapping on direction of curve 2(C2).

6.5 Quantitative analysis

The metric used to quantify the precision of a calibration method is the calibration reproducibility (CR) (Carbajal et al., 2013).

$$CR = \frac{1}{8} \sum_{i=0}^7 |T P_{I,i} - P_{B,i}| \tag{13}$$

Target registration error (TRE)s used to evaluate the accuracy of calibration (Pagoulatos et al., 2001).

$$TRE = \sqrt{\frac{1}{8} \sum_{i=0}^7 |T P_{I,i} - P_{B,i}|^2} \tag{14}$$

Where P_B is the position of test markers in calibration phantom frame.

In the experiment, select a frame image from the image sequence as test image, calculate calibration matrix T using the remaining frame images. The markers in test image is used as the registration target for testing. Quantitative analysis of the dynamic US image calibration is as shown in Table 3.

Compared with other calibration approaches, the comparison results are shown in Table 4.

Table 3 Results of dynamic US image calibration

Number of markers	Calibration P_M (mm)			Physical P_B (mm)			Errors $ P_M - P_B $ (mm)
	x	y	z	x	y	z	
1	72.84	38.25	41.81	72.60	38.11	41.00	1.04
2	65.19	33.31	31.75	65.52	34.40	33.00	1.23
3	58.02	30.39	24.74	58.44	31.68	25.00	1.01
4	51.60	26.43	17.69	51.35	26.96	17.00	0.17
5	-45.29	86.49	56.69	-46.66	86.72	57.00	0.88
6	-41.72	79.41	48.77	-41.93	80.64	49.00	1.16
7	-38.64	72.91	41.43	-38.20	72.56	41.00	0.65
8	-33.39	65.97	34.31	-34.48	65.48	33.00	0.48
							CR 0.83
							TRE 0.89

Table 4 Comparison with other calibration methods

Method	Precision and accuracy of calibration	
	CR (mm)	TRE (mm)
N-wire phantom (Carbajal et al., 2013)	1.97	2.06
Multi-wedge phantom (Najafi et al., 2014)	1.58	1.80
4-D dynamic phantom (proposed method)	0.83	0.89

7 Conclusion

In the experiment, ORB feature extraction method can quickly obtain the accurate pixel of markers in US images and there was no need to denoise the original US image before extracting the marker position. The pixel positions of a total of eight markers could be obtained on the two curves while ensuring that US image was not distorted, which provided data for US probe calibration of the breast intervention robot. The initial parameters (θ , x , y , z) of each marker curve in the calibration can be calculated preliminarily, which provides a foundation for parameter solution of dynamic US probe calibration.

This article demonstrates the feasibility of US probe calibration for a breast intervention robot through experiments and quantity analysis. Specifically, the CR and TRE of the whole system in our proposed method are only 0.83 and 0.89mm, respectively. Those values are far less than the CR (1.97 mm) and TRE (2.06 mm) of the N-wire phantom calibration method and the CR (1.58 mm) and TRE (1.80 mm) of the multi-wedge phantom calibration method. Our proposed 4-D dynamic calibration method is significantly better than the other two image-based methods in terms of the calibration accuracy of the whole system.

Supplementary Information The online version contains supplementary material available at <https://doi.org/10.1007/s10514-022-10055-8>.

Acknowledgements This work was supported by the National Natural Science Foundation of China (Grant No. 61603043).

Declarations

Conflict of interest The authors declare that they have no conflict of interest.

Open Access This article is licensed under a Creative Commons Attribution 4.0 International License, which permits use, sharing, adaptation, distribution and reproduction in any medium or format, as long as you give appropriate credit to the original author(s) and the source, provide a link to the Creative Commons licence, and indicate if changes were made. The images or other third party material in this article are included in the article's Creative Commons licence, unless indicated otherwise in a credit line to the material. If material is not included in the article's Creative Commons licence and your intended use is not permitted by statutory regulation or exceeds the permitted use, you will need to obtain permission directly from the copyright holder. To view a copy of this licence, visit <http://creativecommons.org/licenses/by/4.0/>.

References

- Aalamifar, F., Cheng, A., Kim, Y., Hu, X., Zhang, H. K., Guo, X., & Boctor, E. M. (2016). Robot-assisted automatic ultrasound calibration. *International Journal of Computer Assisted Radiology and Surgery*, 11(10), 1821–1829. <https://doi.org/10.1007/s11548-015-1341-8>
- Carbajal, G., Lasso, A., & GÃşmez, Ã., Fichtinger G. (2013). Improving n-wire phantom-based freehand ultrasound calibration. *International Journal of Computer Assisted Radiology and Surgery*, 8(6), 1063–1072.
- Gupta, S., Kumar, M., & Garg, A. (2019). Improved object recognition results using sift and orb feature detector. *Multimedia Tools and Applications*, 78(23), 34157–34171. <https://doi.org/10.1007/s11042-019-08232-6>
- Huang, Q., Wu, B., Lan, J., & Li, X. (2018). Fully automatic three-dimensional ultrasound imaging based on conventional b-scan. *IEEE Transactions on Biomedical Circuits and Systems*, 12(2), 426–436. <https://doi.org/10.1109/TBCAS.2017.2782815>
- Li, X., Kumar, D., Sarkar, S., & Narayanan, R. (2012). An image registration based ultrasound probe calibration. In: Medical Imaging 2012: Image Processing, February 6, 2012 - February 9, 2012, SPIE, Progress in Biomedical Optics and Imaging - Proceedings of SPIE, vol 8314, pp Agilent Technologies; Diamond SA; DQE Instruments, Inc.; eMagin; et al.; The Society of Photo-Optical Instrumentation Engineers (SPIE), 10.1117/12.911461.
- Najafi, M., Afsham, N., Abolmaesumi, P., & Rohling, R. (2014). A closed-form differential formulation for ultrasound spatial calibration: Multi-wedge phantom. *Ultrasound in Medicine and Biology*, 40(9), 2231–2243. <https://doi.org/10.1016/j.ultrasmedbio.2014.03.006>
- Okwu, M. O., & Tartibu, L. K. (2021) Particle Swarm Optimisation, Springer International Publishing, Cham, pp 5–13. 10.1007/978-3-030-61111-8_2.
- Pagoulatos, N., Haynor, D. R., & Kim, Y. (2001). A fast calibration method for 3-d tracking of ultrasound images using a spatial localizer. *Ultrasound in Medicine and Biology*, 27(9), 1219–1229. [https://doi.org/10.1016/S0301-5629\(01\)00431-8](https://doi.org/10.1016/S0301-5629(01)00431-8)
- Papenberg, N., Lange, T., Modersitzki, J., Schlag, P.M., & Fischer, B. (2008) Image registration for ct and intra-operative ultrasound data of the liver. In: Medical Imaging 2008 - Visualization, Image-Guided Procedures, and Modeling, February 17, 2008 - February 19, 2008, SPIE, Progress in Biomedical Optics and Imaging - Proceedings of SPIE, vol 6918, p The International Society for Optical Engineering (SPIE), 10.1117/12.770105.
- Rublee, E., Rabaud, V., Konolige, K., & Bradski, G. (2011) Orb: An efficient alternative to sift or surf. In: 2011 IEEE International Conference on Computer Vision, ICCV 2011, November 6, 2011 - November 13, 2011, Institute of Electrical and Electronics Engineers Inc., Proceedings of the IEEE International Conference on Computer Vision, pp 2564–2571, 10.1109/ICCV.2011.6126544.
- Solbiati, L., & Tondolo, T. (2013). Imaging of Interventional Therapies in Oncology: Ultrasound, Springer New York, New York, NY, pp 215–230. 10.1007/978-1-4419-0751-6_15.
- Wang, J., Wu, L., Meng, M. Q. H., & Ren, H. (2014) Towards simultaneous coordinate calibrations for cooperative multiple robots. In: 2014 IEEE/RSJ International Conference on Intelligent Robots and Systems, IROS 2014, September 14, 2014 - September 18, 2014, Institute of Electrical and Electronics Engineers Inc., IEEE International Conference on Intelligent Robots and Systems, pp 410–415, 10.1109/IROS.2014.6942592.

- Wang, L., Wang, T., Liu, H., Hu, L., Han, Z., Liu, W., Guo, N., Qi, Y., & Xu, Y. (2018). An automated calibration method of ultrasonic probe based on coherent point drift algorithm. *IEEE Access*, 6, 8657–8665. <https://doi.org/10.1109/ACCESS.2018.2791582>
- Xiong, J., Xu, C., Ibrahim, K., Deng, H., & Xia, Z. (2021). A mechanism-image fusion approach to calibration of an ultrasound-guided dual-arm robotic brachytherapy system. *IEEE/ASME Transactions on Mechatronics*, 26(6), 3211–3220. <https://doi.org/10.1109/TMECH.2021.3055902>
- Yi, Q., Zeng, H., Wu, Y., & Huang, S. (2009). A quaternion-based solution of non-linear 3d coordinate transformation parameters. In: 2009 International Conference on Information Engineering and Computer Science, ICIECS 2009, December 19, 2009 - December 20, 2009, IEEE Computer Society, Proceedings - 2009 International Conference on Information Engineering and Computer Science, ICIECS 2009, p Columbia University; et al.; Huazhong Normal University; National Technology University of Ukraine; Wuhan University; Wuhan University of Technology, 10.1109/ICIECS.2009.5363641.

Publisher's Note Springer Nature remains neutral with regard to jurisdictional claims in published maps and institutional affiliations.